

# High-temperature Ultraviolet Photodetectors: A Review

Ruth A. Miller,<sup>1</sup> Hongyun So,<sup>2</sup> Thomas A. Heuser,<sup>3</sup> and Debbie G. Senesky<sup>1, a)</sup>

<sup>1</sup>Department of Aeronautics and Astronautics  
Stanford University, Stanford, CA 94305, USA

<sup>2</sup>Department of Mechanical Engineering  
Hanyang University, Seoul 04763, Korea

<sup>3</sup>Department of Materials Science and Engineering  
Stanford University, Stanford, CA 94305, USA

## Abstract

Wide bandgap semiconductors have become the most attractive materials in optoelectronics in the last decade. Their wide bandgap and intrinsic properties have advanced the development of reliable photodetectors to selectively detect short wavelengths (i.e., ultraviolet, UV) in high temperature regions (up to 300°C). The main driver for the development of high-temperature UV detection instrumentation is in-situ monitoring of hostile environments and processes found within industrial, automotive, aerospace, and energy production systems that emit UV signatures. In this review, a summary of the optical performance (in terms of photocurrent-to-dark current ratio, responsivity, quantum efficiency, and response time) and uncooled, high-temperature characterization of III-nitride, SiC, and other wide bandgap semiconductor UV photodetectors is presented.

---

<sup>a)</sup> Author to whom correspondence should be addressed. E-mail: dsenesky@stanford.edu

## I. INTRODUCTION

On the electromagnetic spectrum, the ultraviolet (UV) region spans wavelengths from 400 nm to 10 nm (corresponding to photon energies from 3 eV to 124 eV) and is typically divided into three spectral bands: UV-A (400–320 nm), UV-B (320–280 nm), and UV-C (280–10 nm). The Sun is the most significant natural UV source. The approximate solar radiation spectrum just outside Earth's atmosphere, calculated as black body radiation at 5800 K using Planck's law, is shown in Fig. 1. At the top of Earth's atmosphere, about 9% of the Sun's total radiation is in the UV regime [1]. Earth's ozone layer makes the planet habitable by humans by almost completely absorbing UV-C and significantly attenuating UV-B, which causes cataracts, burns, and skin cancer [2]. Artificial sources of UV radiation can be created by passing an electric current through a gas, typically mercury, causing energy to be released in the form of optical radiation. Further information on natural and artificial UV sources can be found in [1].

There are a wide range of ground and space-based applications that require UV detection including optical communication [3], flame detection [4], combustion monitoring [5], chemical analysis [6], astronomy [7], etc. Many of these applications require UV instrumentation capable of operating in high-temperature harsh environments. While most sensors and electronics today are silicon (Si)-based due to well-established manufacturing processes, easy circuit integration, and low cost, Si has shown limited usefulness as a high-temperature UV detecting material platform [8, 9]. Si and other narrow bandgap semiconductors are not able to directly measure UV light due to their bandgaps corresponding to near infrared or visible wavelengths. Since UV light is higher energy than the bandgap of Si and other narrow bandgap materials, part of the energy

will be lost to heating, resulting in low quantum efficiency. To use these materials for UV photodetection, filtering devices that absorb UV light and reemit lower energy light need to be incorporated [10] or detectors with wide, shallow charge collection zones are required since the absorption depth of UV energy in Si is very small (less than 10 nm for wavelengths between 100–300 nm) [11, 12]. Additionally, Si-based photodetectors have been shown to be limited to temperatures less than about 125°C [8, 9]. Si has a relatively high intrinsic carrier concentration at room temperature ( $10^{10} \text{ cm}^{-3}$ ) which increases exponentially with temperature to reach  $10^{15} \text{ cm}^{-3}$  at 300°C [13]. Additionally, the lightest doping concentrations of Si devices range from  $10^{14}$  to  $10^{17} \text{ cm}^{-3}$  [14]. Therefore, when operating at high temperature, the intrinsic carrier concentration will overwhelm the doping concentration and the device will no longer function as intended.

Instead of Si, wide bandgap semiconductors such as III-nitrides, silicon carbide (SiC), and zinc oxide (ZnO) are being explored as material platforms for UV detection. The bandgaps of these materials allow for detection of UV light while remaining blind to visible light. Additionally, electronics based on wide bandgap materials have demonstrated high-temperature operation indicating their applicability to harsh environment sensing [14, 15]. A comparison of the material properties of Si and wide bandgap semiconductors used for UV detection is listed in Table I. Reviews of the latest progress in wide bandgap semiconductor UV photodetectors focusing on new device architectures and novel material combinations have been recently published [11, 16-27]. To complement and expand on these recent reviews, this review presents a summary of the high-temperature characterization and operation of UV photodetectors using wide bandgap semiconductors as well as the challenges that persist in furthering this technology for use in a variety of applications.

## II. PHOTODETECTOR PARAMETERS

There are several types of semiconductor device architectures that can be used to create photodetectors including photoconductor, metal-semiconductor-metal (MSM), Schottky, p-n, p-i-n, and avalanche. A schematic of each device architecture is shown in Fig. 2 and the theoretical framework that describes their operation can be found in [28-30]. Regardless of the photodetector architecture, the basic principal of operation of all semiconductor photodetectors is the same; photons with energy greater than or equal to the bandgap of the semiconductor are absorbed and generate electron-hole pairs. Under an applied electric field the electron-holes pairs separate and a photo-generated current can be measured. The main figures of merit that are used to quantify photodetector performance are photocurrent-to-dark current ratio (PDCR), responsivity (R), quantum efficiency ( $\eta$ ), and response time.

PDCR is a measure of the photodetector sensitivity with respect to the dark (or leakage) current. PDCR is defined as

$$PDCR = \frac{I_{photo} - I_{dark}}{I_{dark}} \quad (1)$$

where  $I_{photo}$  is the measured photocurrent and  $I_{dark}$  is the dark current. Responsivity is another measure of photodetector sensitivity and is defined as the photo-generated current ( $I_{photo} - I_{dark}$ ) per unit of incident optical power, that is

$$R = \frac{I_{photo} - I_{dark}}{P_{opt}} \quad (2)$$

where  $P_{opt}$  is the applied optical power. Responsivity is directly proportional to the external quantum efficiency ( $\eta$ ) which is a measure of the number of photo-generated electron-hole pairs per incident photon. The external quantum efficiency is defined as

$$\eta = R \frac{hc}{q\lambda} \quad (3)$$

where  $h$  is Plank's constant,  $c$  is the speed of light,  $q$  is elementary charge, and  $\lambda$  is wavelength. Photodetector response time (which is related to bandwidth) is quantified in terms of photocurrent 10% to 90% rise time and photocurrent 90% to 10% decay time.

A comparison of the maximum operational temperatures reported in literature for Si, SiC, III-nitride, and other wide bandgap-based UV photodetectors is shown in Fig. 3. To date, SiC-based photodetectors have demonstrated the highest operational temperatures, up to 550°C [31]. The following sections detail the high temperature photodetector response in terms of PDCR,  $R$ ,  $\eta$ , and response time for each of these material platforms. Additionally, the development and continuing challenges of using wide bandgap semiconductors for high temperature UV sensing are discussed.

### III. III-NITRIDE-BASED UV PHOTODETECTORS

The III-nitrides, consisting of GaN, InN, AlN, and their ternary compounds, present some unique benefits for UV photodetection when compared to other wide bandgap materials. III-nitride semiconductors have direct bandgaps and thus higher photon absorption than their indirect counterparts (such as Si or SiC). Also, the region of the electromagnetic spectrum, between 200 nm (AlN, bandgap of 6.2 eV) and 650 nm (InN, bandgap of 1.9 eV), that III-nitride

detectors are sensitive to can be selected by changing the ternary compound mole fraction [11, 16]. Lastly, heterojunctions can be formed from III-nitride semiconductors and the highly conductive two-dimensional electron gas (2DEG) formed at the material interface can be leveraged as a photo-sensing element [32-35].

On the other hand, III-nitride materials have some limitations when used for UV sensing, the most significant of which is known as persistent photoconductivity (PPC). PPC is a phenomenon in which the photocurrent response remains after the illumination source has been removed as shown in Fig. 4, resulting in photocurrent decay times on the order of hours to days [32, 35-41]. PPC has been attributed to excitons [32], negatively charged surface states [38], metastable defects [37, 39, 40], gallium vacancies [36, 39], nitrogen antisites [40], and deep-level defects [39, 41] trapping photo-generated carriers. The falling transient is often fit by a stretched exponential function of the form

$$I_{PPC}(t) = I_0 \exp \left[ - \left( \frac{t}{\tau} \right)^\beta \right] \quad (4)$$

where  $I_0$  is the photocurrent before the illumination source is removed,  $\tau$  is the decay time constant, and  $\beta$  is the decay exponential ( $0 < \beta < 1$ ) [36, 39-42]. Experimental results have shown that at elevated temperatures, thermal energy is able to release trapped photo-generated carriers and thus reduce PPC effects [32, 35, 37]. To account for this temperature dependence, the decay time constant has been modeled as

$$\tau = \tau_0 \exp \left( \frac{\Delta E}{kT} \right) \quad (5)$$

where  $\Delta E$  is the carrier capture barrier,  $k$  is Boltzmann's constant, and  $T$  is the temperature [37, 40, 43]. The carrier capture barrier is thought to originate from the non-overlapping vibronic states of unfilled and filled defects [44]. To be captured, charge carriers require additional energy to get into the vibronic states of filled defects. Reported values for  $\Delta E$  in III-nitride photodetectors range from 132 meV to 360 meV [35, 37, 40, 41]. This large energy barrier prevents the decay of photo-generated carriers at low temperatures. However, as trapped carriers gain thermal energy at elevated temperatures, the capture rate increases and thus the decay time is reduced.

In addition to increasing the photocurrent decay time, trapped charge carriers also affect photodetector quantum efficiency. Room temperature quantum efficiencies greater than 100% are often reported for III-nitride-based photodetectors and attributed to a photo-gain mechanism [38, 45-49]. The photo-gain has been attributed to photo-generated holes trapped at negatively-charged surface states at the metal-semiconductor interface causing the Schottky barrier to lower or bend with respect to the dark Schottky barrier as shown in Fig. 5 [38, 48, 49]. This change in the Schottky barrier results in an enhanced leakage current. Similar to PPC, thermal energy is able to release trapped photo-generated holes [46, 48]. Therefore, at elevated temperatures the change in the Schottky barrier from dark to illuminated conditions is less pronounced resulting in minimal photo-gain. In addition to a reduced photo-gain at high temperature, increased dark (or leakage) current, enhanced carrier recombination, increased lattice scattering, and shifting of the bandgap to longer wavelengths have been cited as reasons for lower quantum efficiencies, responsivities, and PDCRs at elevated temperatures [32, 33, 50, 51]. Increased responsivity at higher temperatures has also been reported and has been attributed to thermal ionization of trapped photo-generated carriers providing additional carriers [32, 45, 52].

Table II details the high temperature performance of III-nitride-based photodetectors reported in literature. The highest reported operational temperature of any III-nitride-based photodetector is 327°C by an AlGaIn/GaN MSM device [32]. However, this photodetector exhibited decay times more than a factor of two greater than a similar MSM photodetector fabricated on a GaN substrate [32]. These long decay times were attributed to a high defect density as determined from surface roughness measurements. Thus, to reduce PPC effects, high quality III-nitride films are needed. Thicker GaN films have been shown to contain fewer defects and indeed, MSM photodetectors on a 4.0 μm thick GaN film showed improved performance compared to photodetectors fabricated on 1.5 μm thick GaN film [53].

Aside from growing higher quality, less defective III-nitride films, another proposed approach to mitigate PPC effects is to use in situ heating. Suspended AlGaIn/GaN photodetectors utilizing the 2DEG as both a sensor and heater demonstrated a photocurrent decay time of 24 seconds which was more than three orders of magnitude less than the 39 hour decay time of their solid state counterpart [35]. The suspended photodetectors used joule heating of the 2DEG to accelerate the carrier capture rate once the UV source was removed which successfully mitigated PPC effects.

To increase quantum efficiency, PDCR, and responsivity at high temperatures, thermally stable contacts with low dark current are needed. To accomplish this, calcium fluoride (CaF<sub>2</sub>) was tested as an insulation layer in InGaIn-based metal-insulator-semiconductor (MIS) Schottky photodiodes [45, 52]. Compared to the commonly used SiO<sub>2</sub> insulation layer, CaF<sub>2</sub> has an extremely wide bandgap (12 eV), high thermal conductivity, and is robust to radiation [52]. The addition of the CaF<sub>2</sub> insulation layer decreased the reverse leakage current by three orders of magnitude compared to Schottky photodiodes without the insulation layer [45, 52]. The MIS



device demonstrated operation up to 250°C with a PDCR values of 1317 at room temperature and 72 at 250°C [45, 52]. Whereas Schottky photodiodes without the insulation layer were only operational up to 200°C with lower PDCRs of 79 at room temperature and 2.2 at 200°C [45, 52].

Another approach to increase quantum efficiency, PDCR, and responsivity at high temperatures is to increase the UV light absorption. Three-dimensional AlGaIn/GaN UV photodetectors using a “v-grooved” Si substrate demonstrated operation up to 200°C with improved PDCR over planar AlGaIn/GaN UV photodetectors (~1.4 compared to ~0.9 at room temperature and ~0.3 compared to ~0.1 at 200°C ) [33]. The increased sensitivity was attributed to the increased absorption (via redirection of reflected light) of the incident UV light in the three-dimensional substrate. III-nitride photodetectors with ZnO nanorod arrays have also demonstrated enhanced sensitivity at high temperatures due to their anti-reflective properties [54]. Increased photodetector sensitivity due to ZnO nanorod arrays was demonstrated with a direct wirebond photodetector where a GaN chip was directly wirebonded to a carrier chip thus avoiding time consuming and costly microfabrication steps such as photolithography, metal sputtering (or evaporation), and etching (or lift-off) [54]. These rapidly fabricated/package photodetectors had a PDCR of 1.11 at room temperature and demonstrated operation up to 250°C with a PDCR of 0.11. With the addition of an anti-reflective ZnO nanorod array coating to enhance light trapping, the direct wirebond photodetector sensitivity improved to 2.63 and 0.27 at room temperature and 250°C, respectively [54].

Lastly, few reports of AlN photodetectors have been published. However, AlN is a promising material candidate for high temperature deep-UV (< 200 nm) sensing applications. AlN has a bandgap of 6.2 eV which corresponds to a cut-off wavelength of 200 nm, making AlN photodetectors not only visible blind but also solar blind. MSM photodetectors fabricated on AlN

thin films grown on a Si substrate demonstrated room temperature dark currents below 1 nA at applied bias voltages up to 200 V and room temperature PDCRs as high as 63 [55]. The AlN photodetectors demonstrated operation up to 300°C (PDCR of 3.5) and the room temperature response was fully recovered after thermal cycling up to 400°C [55].

#### IV. SiC-BASED UV PHOTODETECTORS

SiC is another attractive wide bandgap semiconductor for UV detection at high temperatures. In particular, 4H-SiC has strong chemical bonds, high thermal conductivity ( $4\text{--}4.9\text{ W}\cdot\text{cm}^{-1}\cdot\text{K}^{-1}$ ) [58], and high electron saturation velocity ( $2.7\times 10^7\text{ cm}\cdot\text{s}^{-1}$ ) [59] enabling 4H-SiC based UV photodetectors to operate in high-temperature and high-radiation environments with fast response speed. Table III summarizes the type (structure) of device, electrode metal, operation temperature, PDCR, and responsivity of SiC-based UV photodetectors. The average operation temperature is slightly higher than the operation temperature of GaN-based UV photodetectors while the overall values of responsivity are relatively smaller than those of GaN-based photodetectors. The highest reported operational temperature of SiC-based photodetectors is 550°C by p-i-n structure [31]. From room temperature to 550°C, the photocurrent increased by 9 times at 365 nm and decreased by 2.6 times at 275 nm due to bandgap narrowing effect at high temperature as shown in Fig. 6 [31, 60]. This thermally-induced bandgap narrowing effect also induces an increase in the optical absorption coefficient [61, 62], thus increasing the quantum efficiency of photodetectors as temperature increases. Based on this effect, the highest quantum efficiency of 53.4% and 63.6% was reported at room temperature and 150°C, respectively, by 4H-SiC avalanche photodiodes [63]. For long-term reliability at high temperature, a 4H-SiC photodetector using Schottky metal contacts was exposed to 200°C in air for 100 hours [64].

After thermal storage, the responsivity and dark current level of the device remained unchanged, thus indicating the reliable operation of 4H-SiC UV photodetectors at high temperatures up to 200°C [64]. The temperature-independent responsivity of SiC photodetectors was also studied since the photoresponse usually depends on temperature. By controlling the reverse-bias voltage from 0 to 150 V, 4H-SiC p-n photodiodes were shown to have temperature-independent responsivity under 280–300 nm wavelength range as shown in Fig. 7 [65]. This phenomenon was explained by a combination of temperature-dependent optical absorption coefficient and surface recombination effects [65].

Compared to GaN-based photodetectors, severe PPC effect was not observed in SiC-based photodetectors which enables photodiodes to have a fast response time. The rise/fall time of an MSM photodetector using 7  $\mu\text{m}$  p-type 4H-SiC epitaxial layer was reported as 594  $\mu\text{s}$ /699  $\mu\text{s}$  and 684  $\mu\text{s}$ /786  $\mu\text{s}$  at room temperature and 400°C, respectively [8]. Because the bandwidth of 4H-SiC is decreased due to the decrease in hole/electron saturation velocity as temperature increases, the rise/fall time of the photodetector is slightly increased at high temperature [8]. Although many SiC-based photodetectors are fabricated on 4H-SiC epitaxial layer, 6H-SiC [66], nanocrystalline SiC [67], and  $\beta$ -SiC (or 3C-SiC) [68] have also been used for fabrication of UV photodetectors. In particular,  $\beta$ -SiC on Si substrate was used to obtain high gain of optical sensor [68]. To extend the operation temperature and improve the high temperature performance, porous silicon substrate was additionally adopted as the semi-insulating substrate, suppressing the leakage current and thus resulting in a low dark current level [68]. The synthesis of ZnO nanorod arrays (i.e., antireflective coating) on SiC layer was reported as an alternative method to increase the operation temperature of the photodetectors [67].

## V. OTHER TYPES OF UV PHOTODETECTORS

In addition to GaN and SiC as discussed above, there are other less developed materials with bandgaps appropriate for ultraviolet photodetection that are also capable of operating at elevated temperatures including zinc oxide (ZnO), gallium oxide ( $\text{Ga}_2\text{O}_3$ ), diamond, and boron nitride (BN) [24-27]. To date, a  $\text{Ga}_2\text{O}_3$  MSM photodetector with transparent indium zinc oxide (IZO) electrodes has the highest reported operating temperature ( $427^\circ\text{C}$ ) of all photodetectors based on these other materials [71]. Table IV details the reported operating temperatures of photodetectors based on these materials with the benefits and drawbacks each material discussed further below.

ZnO, a II-VI semiconductor, is often compared to GaN. Both preferentially form in the wurtzite crystal structure, and they have direct band gaps with very similar energies (3.37 eV vs. 3.4 eV for GaN, corresponding to a cut-off wavelength of 368 nm) [72]. This, combined with a high decomposition temperature ( $\sim 1975^\circ\text{C}$ ), means that ZnO is very well suited for use in high-temperature UV photodetectors. Although ZnO has been studied extensively as a material for UV photodetection, there has been little investigation into the behavior of ZnO-based devices at elevated temperatures, with the highest reported testing (of an MSM device with Al electrodes) carried out at  $200^\circ\text{C}$  [72]. Operation at this temperature showed reduced photocurrent and responsivity, as well as increased dark current compared with samples tested at room temperature. These changes were attributed to band gap shrinkage and increased lattice scattering [72].

$\beta\text{-Ga}_2\text{O}_3$ , with a band gap of 4.9 eV (253 nm), is the most stable of the five polymorphs of  $\text{Ga}_2\text{O}_3$ . It has a melting point of  $\sim 1780^\circ\text{C}$  ( $\alpha\text{-Ga}_2\text{O}_3$  has a higher theoretical melting point of  $\sim 1900^\circ\text{C}$  but transforms into  $\beta\text{-Ga}_2\text{O}_3$  at temperatures over  $800^\circ\text{C}$ ) [73]. Much of the interest in

$\beta$ -Ga<sub>2</sub>O<sub>3</sub> stems from its potential as a transparent conducting oxide (TCO) that allows for transmission of long-wavelength ultraviolet light, a result of its large band gap [74]. A variety of  $\beta$ -Ga<sub>2</sub>O<sub>3</sub> UV photodetectors (mostly Schottky diodes, and MSM devices) have been tested at elevated temperatures, and are particularly notable for their short decay times, extremely low dark currents, and solar-blind photoresponses [71, 75-78].  $\beta$ -Ga<sub>2</sub>O<sub>3</sub> UV photodetectors have also demonstrated robustness through little variation in device behavior with changing atmospheric oxygen concentration and good resistance to permanent degradation at elevated temperatures, with one device (MSM with IZO electrodes) showing full recovery of room-temperature behavior after testing at 427°C, the current high-temperature record for  $\beta$ -Ga<sub>2</sub>O<sub>3</sub> UV photodetectors [71].

Diamond has a band gap of ~ 5.5 eV (225 nm), is one of the hardest known materials, has a very high (pressure-dependent) theoretical sublimation temperature (over 3000°C), but readily transforms into graphite at temperatures above ~1200°C. (Diamond is thermodynamically unstable with respect to graphite at all temperatures, but the transformation is extremely slow at lower temperatures) [79]. Pure diamond is often doped (particularly with boron) to improve its semiconducting properties [80]. MSM photodetectors fabricated on 1  $\mu$ m-thick polycrystalline CVD-deposited diamond films with Ag electrodes have been tested up to 300°C, displaying a responsivity of over 100 mA/W for the range from 225-350 nm [81].

Hexagonal boron nitride (h-BN) has a band gap of ~6 eV (206 nm) corresponding to the deep ultraviolet and is particularly notable, even among wide-band gap semiconductors, for its high decomposition temperature (2,973°C). Due to its extremely wide bandgap, h-BN is solar-blind and therefore does not need solar rejection filters to operate in the deep ultraviolet [82]. H-BN can be synthesized in a variety of forms including nanorods, nanotubes, and nanosheets

(BNNS) with 2D nanosheets of special interest due to their physical and structural similarities (in addition to thermal stability) to graphene [83]. Photodetectors based on BNNS with Au electrodes tested up to 400°C displayed a factor of four increase in photocurrent and a factor of three increase in thermal noise compared to devices tested at room temperature [82, 83]. This combination of high photocurrent, solar-blind photoresponse, and high thermal stability mean that BNNS is particularly well suited to use in high-temperature ultraviolet photodetectors.

## **VI. CONCLUSIONS**

Wide bandgap semiconductors have advanced high temperature UV sensing beyond the capabilities of silicon due to their intrinsic thermal stability. Of the wide bandgap semiconductors used for high temperature UV detection, the III-nitrides and SiC are the most developed and have demonstrated operating temperatures upwards of 300°C. However, further development of all of these material platforms is needed to enable high UV sensitivity with long term reliable operation at elevated temperatures. For these materials to reach their full potential, material quality issues need to be addressed, high temperature capable electrode technology needs to be furthered, and high temperature packaging schemes need to be developed.

## **AUTHOR INFORMATION**

### **Corresponding Authors**

\*E-mail: dsenesky@stanford.edu

## References

- (1) B. L. Diffey, "Sources and measurement of ultraviolet radiation," *Methods*, vol. 28, no. 1, pp. 4-13, Sept. 2002.
- (2) H. K. Biesalski and U. C. Obermueller-Jevic, "UV light, beta-carotene and human skin-beneficial and potentially harmful effects," *Archives of Biochemistry and Biophysics*, vol. 389, no. 1, pp. 1-6, May 2001.
- (3) Z. Xu and B. M. Sadler, "Ultraviolet communications: Potential and state-of-the-art," *IEEE Communications Magazine*, vol. 46, no. 5, pp. 67-73, May 2008.
- (4) T. Oshima, T. Okuno, N. Arai, N. Suzuki, H. Hino, and S. Fujita, "Flame detection by a b-Ga<sub>2</sub>O<sub>3</sub>-based sensor," *Japanese Journal of Applied Physics*, vol. 48, p. 011605, Jan. 2009.
- (5) J. L. Pau, J. Anduaga, C. Rivera, A. Navarro, I. Alava, M. Redondo, and E. Munoz, "Optical sensors based on III-nitride photodetectors for flame sensing and combustion monitoring," *Applied Optics*, vol. 45, no. 28, pp. 7498-7503, Oct. 2006.
- (6) J. Golimowski and K. Golimowska, "UV-photooxidation as pretreatment step in inorganic analysis of environmental samples," *Analytica Chimica Acta*, vol. 325, no. 3, pp. 111-133, May 1996.
- (7) J. L. Robichaud, "SiC optics for EUV, UV, and visible space missions," Proceedings of SPIE 4854, pp. 39-49, 2003, <http://dx.doi.org/10.1117/12.459771>.
- (8) W.-C. Lien, D.-S. Tsai, D.-H. Lien, D. G. Senesky, J.-H. He, and A. P. Pisano, "4H-SiC metal-semiconductor-metal ultraviolet photodetectors in operation of 450°C," *IEEE Electron Device Letters*, vol. 33, no. 11, pp. 1586-1588, Nov. 2012.

- (9) A. Vijayakumar, R. M. Todi, and K. B. Sundaram, "Amorphous-SiCBN-based metal-semiconductor-metal photodetector for high-temperature applications," *IEEE Electron Device Letters*, vol. 28, no. 8, pp. 713-715, Aug. 2007.
- (10) D. Decoster and J. Harari, "Ultraviolet Photodetectors," in *Optoelectronic Sensors*. Hoboken, NJ: John Wiley & Sons, Inc., 2009, pp. 181-222.
- (11) Z. Alaie, S. Mohammad Nejad, and M. H. Yousefi, "Recent advances in ultraviolet photodetectors," *Materials Science in Semiconductor Processing*, vol. 29, pp. 16-55 Jan. 2015.
- (12) L. Shi and S. Nihtianov, "Comparative study of silicon-based ultraviolet photodetectors," *IEEE Sensors Journal*, vol. 12, no. 7, pp. 2453-2459, Apr. 2012.
- (13) R. F. Pierret, *Semiconductor Device Fundamentals*. Boston, MA: Addison-Wesley, 1996.
- (14) P. G. Neudeck, R. O. Okojie, and L.-Y. Chen, "High-temperature electronics – a role for wide bandgap semiconductors?," *Proceedings of the IEEE*, vol. 90, no. 6, pp. 1065-1076, Nov. 2002.
- (15) C. Buttay, D. Planson, B. Allard, D. Bergogne, P. Bevilacqua, C. Joubert, M. Lazar, C. Martin, H. Morel, D. Tournier, C. Raynaud, "State of the art of high temperature power electronics," *Materials Science and Engineering B*, vol. 176, no. 4, pp. 283-288, Mar. 2011.
- (16) E. Monroy, F. Omnes, and F. Calle, "Wide-bandgap semiconductor ultraviolet photodetectors," *Semiconductor Science and Technology*, vol. 18, no. 4, pp. R33-R51, Apr. 2003.



- (17) L. Sang, M. Liao, and M. Sumiya, "A comprehensive review of semiconductor ultraviolet photodetectors: from thin film to one-dimensional nanostructures," *Sensors*, vol. 13, no. 8, pp. 10482-10518, Aug. 2013.
- (18) M. Razeghi and A. Rogalski, "Semiconductor ultraviolet detectors," *Journal of Applied Physics*, vol. 79, no. 10, pp. 7433-7473, May 1996.
- (19) E. Munoz, E. Monroy, J. L. Pau, F. Calle, F. Omnes, and P. Gibart, "III nitrides and UV detection," *Journal of Physics: Condensed Matter*, vol. 13, pp. 7115-7137, July 2001.
- (20) C. Rivera, J. Pereiro, A. Navarro, E. Munoz, O. Brandt, and H. T. Grahn, "Advances in group-III-nitride photodetectors," *The Open Electrical & Electronic Engineering Journal*, vol. 4, pp. 1-9, May 2010.
- (21) E. Monroy, F. Calle, J. L. Pau, E. Munoz, F. Omnes, B. Beaumont, and P. Gibart, "AlGaIn-based UV photodetectors," *Journal of Crystal Growth*, vol. 230, no. 3-4, pp. 537-543, Sep. 2001.
- (22) T. D. Moustakas and R. Paiella, "Optoelectronic device physics and technology of nitride semiconductors from the UV to the terahertz," *Reports on Progress in Physics*, vol. 80, p. 106501, Sep. 2017.
- (23) F. Omnes and E. Monroy, "GaN-based UV photodetectors," in *Nitride Semiconductors: Handbook on Materials and Devices*. Weinheim, Germany: Wiley-VCH Verlag GmbH & Co., 2003, pp. 627-660.
- (24) K. Liu, M. Sakurai, and M. Aono, "ZnO-based ultraviolet photodetectors," *Sensors*, vol. 10, no. 9, pp. 8604-8634, Sep. 2010.
- (25) H. Chen, K. Liu, L. Hu, A. A. Al-Ghamdi, and X. Fang, "New concept ultraviolet photodetectors," *Materials Today*, vol. 18, no. 9, pp. 493-502, Nov. 2015.

- (26) G. Konstantatos and E. H. Sargent, "Nanostructured materials for photon detection," *Nature Nanotechnology*, vol. 5, pp. 391-400, May 2010.
- (27) L. Peng, L. Hu, and X. Fang, "Low-dimensional nanostructure ultraviolet photodetectors," *Advanced Materials*, vol. 25, no. 37, pp. 5321-5328, Oct. 2013.
- (28) S. M. Sze, and K. K. Ng, *Physics of Semiconductor Devices*, 3<sup>rd</sup> Ed. Hoboken, NJ: John Wiley & Sons, Inc., 2007.
- (29) S. M. Sze, D. J. Coleman Jr., and A. Loya, "Current transport in metal-semiconductor-metal (MSM) structures," *Solid-State Electronics*, vol. 14, no. 12, pp. 1209-1218, Dec. 1971.
- (30) P. Bhattacharya, *Semiconductor Optoelectronic Devices*, 2<sup>nd</sup> Ed. Hoboken, NJ: Prentice Hall, 1997.
- (31) S. Hou, P.-E. Hellstrom, C.-M. Zetterling, and M. Ostling, "550°C 4H-SiC p-i-n photodiode array with two-layer metallization," *IEEE Electron Device Letters*, vol. 37, no. 12, p. 1594-1596, Dec. 2016.
- (32) M. De Vittorio, B. Poti, M. T. Todaro, M. C. Frassanito, A. Pomarico, A. Passaseo, M. Lomascolo, and R. Cingolani, "High temperature characterization of GaN-based photodetectors," *Sensors and Actuators A*, vol. 113, no. 3, pp. 329-333, Aug. 2004.
- (33) H. So, J. Lim, and D. G. Senesky, "Continuous V-grooved AlGaIn/GaN surfaces for high-temperature ultraviolet photodetectors," *IEEE Sensors Journal*, vol. 16, no. 10, pp. 3633-3639, May 2016.

- (34) H. So and D. G. Senesky, "Rapid fabrication and packaging of AlGa<sub>N</sub>/Ga<sub>N</sub> high-temperature ultraviolet photodetectors using direct wire bonding," *Journal Physics D: Applied Physics*, vol. 49, no. 28, p. 285109, June 2016.
- (35) M. Hou, H. So, A. J. Suria, A. S. Yalamarthy, and D. G. Senesky, "Suppression of persistent photoconductivity in AlGa<sub>N</sub>/Ga<sub>N</sub> ultraviolet photodetectors using in situ heating," *IEEE Electron Device Letters*, vol. 38, no. 1, pp. 56-59, Jan. 2017.
- (36) B. Poti, A. Passaseo, M. Lomascolo, R. Cingolani, and M. De Vittorio, "Persistent photocurrent spectroscopy of Ga<sub>N</sub> metal-semiconductor-metal photodetectors on long time scale," *Applied Physics Letters*, vol. 85, no. 25, pp. 6083-6085, Oct. 2004.
- (37) M. T. Hirsch, J. A. Wolk, W. Walukiewicz, and E. E. Haller, "Persistent photoconductivity in n-type Ga<sub>N</sub>," *Applied Physics Letters*, vol. 71, no. 8, pp. 1098-1100, June 1997.
- (38) O. Katz, G. Bahir, and J. Salzman, "Persistent photocurrent and surface trapping in Ga<sub>N</sub> Schottky ultraviolet detectors," *Applied Physics Letters*, vol. 84, no. 20, pp. 4092-4094, May 2004.
- (39) C. H. Qiu and J. I. Pankove, "Deep levels and persistent photoconductivity in Ga<sub>N</sub> thin films," *Applied Physics Letters*, vol. 70, no. 15, pp. 1983-1985, Feb. 1997.
- (40) H. M. Chen, Y. F. Chen, M. C. Lee, and M. S. Feng, "Persistent photoconductivity in n-type Ga<sub>N</sub>," *Journal of Applied Physics*, vol. 82, no. 2, pp. 899-901, July 1997.
- (41) J. Z. Li, J. Y. Lin, H. X. Jiang, M. Asif Khan, and Q. Chen, "Persistent photoconductivity in a two-dimensional electron gas system formed by an AlGa<sub>N</sub>/Ga<sub>N</sub> heterostructure," *Journal of Applied Physics*, vol. 82, no. 3, pp. 1227-1230, Apr. 1997.

- (42) X. Z. Dang, C. D. Wang, E. T. Yu, K. S. Boutros, and J. M. Redwing, "Persistent photoconductivity and defect levels in n-type AlGaIn/GaN heterostructures," *Applied Physics Letters*, vol. 72, no. 21, pp. 2745-2747, Feb. 1998.
- (43) J. Z. Li, J. Y. Lin, H. X. Jiang, A. Salvador, A. Botchkarev, and H. Morkoc, "Nature of Mg impurities in GaN," *Applied Physics Letters*, vol. 69, no. 10, pp. 1474-1476, June 1996.
- (44) D. V. Lang and R. A. Logan, "Large-lattice-relaxation model for persistent photoconductivity in compound semiconductors," *Physical Review Letters*, vol. 39, no. 10, pp. 635-639, Sep. 1977.
- (45) L. Sang, M. Liao, Y. Koide, and M. Sumiya, "High-temperature ultraviolet detection based on InGaIn Schottky photodiodes," *Applied Physics Letters*, vol. 99, no. 3, p. 031115, July 2011.
- (46) E. Munoz, E. Monroy, J. A. Garrido, I. Izpura, F. J. Sanchez, M. A. Sanchez-Garcia, E. Calleja, B. Beaumont, and P. Gibart, "Photoconductor gain mechanisms in GaN ultraviolet detectors," *Applied Physics Letters*, vol. 71, no. 7, pp. 870-872, June 1997.
- (47) F. Binet, J. Y. Duboz, E. Rosencher, F. Scholz, and V. Harle, "Mechanisms of recombination in GaN photodetectors," *Applied Physics Letters*, vol. 69, no. 9, pp. 1202-1204, Aug. 1996.
- (48) F. Xie, H. Lu, X. Xiu, D. Chen, P. Han, R. Zhang, and Y. Zheng, "Low dark current and internal gain mechanism of GaN MSM photodetectors fabricated on bulk GaN substrate," *Solid-State Electronics*, vol. 57, no. 1, pp. 39-42, Mar. 2011.
- (49) L. Liu, C. Yang, A. Patane, Z. Yu, F. Yan, K. Wang, H. Lu, J. Li, and L. Zhao, "High-detectivity ultraviolet photodetectors based on laterally mesoporous GaN," *Nanoscale*, vol. 9, no. 24, pp. 8142-8148, Mar. 2017.

- (50) S. Chang, M. Chang, and Y. Yang, "Enhanced responsivity of GaN metal-semiconductor-metal (MSM) photodetectors on GaN substrate," *IEEE Photonics Journal*, vol. 9, no. 2, p. 6801707, Apr. 2017.
- (51) F. Xie, H. Lu, D. Chen, X. Ji, F. Yan, R. Zhang, Y. Zheng, L. Li, and J. Zhou, "Ultra-low dark current AlGaIn-based solar-blind metal-semiconductor-metal photodetectors for high-temperature applications," *IEEE Sensors Journal*, vol. 12, no. 6, pp. 2086-2090, June 2012.
- (52) L. W. Sang, M. Y. Liao, Y. Koide, and M. Sumiya, "InGaIn photodiodes using CaF<sub>2</sub> insulator for high-temperature UV detection," *Physica Status Solidi C*, vol. 9, no. 3-4, pp. 953-956, Mar. 2012.
- (53) J. C. Carrano, T. Li, P. A. Grudowski, C. J. Eiting, R. D. Dupuis, and J. C. Campbell, "Current transport mechanisms in GaN-based metal-semiconductor-metal photodetectors," *Applied Physics Letters*, vol. 72, no. 5, pp. 542-544, Dec. 1998.
- (54) H. So, and D. G. Senesky, "ZnO nanorod arrays and direct wire bonding on GaN surfaces for rapid fabrication of antireflective, high-temperature ultraviolet sensors," *Applied Surface Science*, vol. 387, pp. 280-284, Nov. 2016.
- (55) D.-S. Tsai, W.-C. Lien, D.-H. Lien, K.-M. Chen, M.-L. Tsai, D. G. Senesky, Y.-C. Yu, A. P. Pisano, and J.-H. He, "Solar-blind photodetectors for harsh electronics," *Scientific Reports*, vol. 3, p. 2628, Sep. 2013.
- (56) F. Xie, H. Lu, D. Chen, R. Zhang, and Y. Zheng, "GaN MSM photodetectors fabricated on bulk GaN with low dark-current and high UV/visible rejection ratio," *Physica Status Solidi C*, vol. 8, no. 7-8, pp. 2473-2475, Apr. 2011.

- (57) G. Wang, F. Xie, H. Lu, D. Chen, R. Zhang, Y. Zheng, L. Li, and J. Zhou, "Performance comparison of front- and back-illuminated AlGa<sub>N</sub>-based metal-semiconductor-metal solar-blind ultraviolet photodetectors," *Journal of Vacuum Science and Technology B*, vol. 31, no. 1, p. 011202, Nov. 2013.
- (58) S. E. Saddow and A. Agarwal, *Advances in Silicon Carbide Processing and Applications*, Norwood, MA: Artech House, 2004.
- (59) R. P. Joshi, "Monte Carlo calculations of the temperature- and field-dependent electron transport parameters for 4H-SiC," *Journal of Applied Physics*, vol. 78, no. 9, pp. 5518-1521, Nov. 1995.
- (60) M. Mazzillo, A. Sciuto, and S. Marchese, "Impact of the epilayer doping on the performance of thin metal film Ni<sub>2</sub>Si/4H-SiC Schottky photodiodes," *Journal of Instrumentation*, vol. 9, p. P12001, Dec. 2014.
- (61) H. Y. Cha, S. Soloviev, S. Zelakiewicz, P. Waldrab, and P. M. Sandvik, "Temperature dependent characteristics of nonreach-through 4H-SiC separate absorption and multiplication APDs for UV detection," *IEEE Sensors Journal*, vol. 8, no. 3, pp. 233-237, Jan. 2008.
- (62) D. M. Brown, E. T. Downey, M. Ghezzi, J. W. Kretchmer, R. J. Saia, Y. S. Liu, J. A. Edmond, G. Gati, J. M. Pimbley, and W. E. Schneider, "Silicon carbide UV photodiodes," *IEEE Transactions on Electron Devices*, vol. 40, no. 2, pp. 325-333, Feb. 1993.
- (63) D. Zhou, F. Liu, H. Lu, D. Chen, F. Ren, R. Zhang, and Y. Zheng, "High-temperature single photon detection performance of 4H-SiC avalanche photodiodes," *IEEE Photonics Technology Letters*, vol. 26, no. 11, pp. 1136-1138, June 2014.

- (64) Y. Xu, D. Zhou, H. Lu, D. Chen, F. Ren, R. Zhang, and Y. Zheng, "High-temperature and reliability performance of 4H-SiC Schottky-barrier photodiodes for UV detection," *Journal of Vacuum Science and Technology B*, vol. 33, no. 4, p. 040602, June 2015.
- (65) N. Watanabe, T. Kimoto, and J. Suda, "4H-SiC pn photodiodes with temperature-independent photoresponse up to 300°C," *Applied Physics Express*, vol. 5, p. 094101, Aug. 2012.
- (66) Y. Ueda, S. Akita, Y. Nomura, Y. Nakayama, and H. Naito, "Study of high temperature photocurrent properties of 6H-SiC UV sensor," *Thin Solid Films*, vol. 517, no. 4, pp. 1471-1473, Dec. 2008.
- (67) W.-C. Lien, D.-S. Tsai, S.-H. Chiu, D. G. Senesky, R. Maboudian, A. P. Pisano, and J.-H. He, "Low-temperature, ion beam-assisted SiC thin films with antireflective ZnO nanorod arrays for high-temperature photodetection," *IEEE Electron Device Letters*, vol. 32, no. 11, pp. 1564-1566, Nov. 2011.
- (68) W. T. Hsieh, Y. K. Fang, K. H. Wu, W. J. Lee, J. J. Ho, and C. W. Ho, "Using porous silicon as semi-insulating substrate for  $\beta$ -SiC high temperature optical-sensing devices," *IEEE Transactions on Electron Devices*, vol. 48, no. 4, pp. 801-803, Apr. 2001.
- (69) X. Bai, X. Guo, D. C. McIntosh, H.-D. Liu, and J. C. Campbell, "High detection sensitivity of ultraviolet 4H-SiC avalanche photodiodes," *IEEE Journal of Quantum Electronics*, vol. 43, no. 12, pp. 1159-1163, Dec. 2007.
- (70) T. V. Blank, Y. A. Goldberg, E. V. Kalinina, O. V. Konstantinov, A. O. Konstantinov, and A. Hallen, "Temperature dependence of the photoelectric conversion quantum efficiency of 4H-SiC Schottky UV photodetectors," *Semiconductor Science and Technology*, vol. 20, no. 8, pp. 710-715, May 2005.

- (71) T.-C. Wei, D.-S. Tsai, P. Ravadgar, J.-J. Ke, M.-L. Tsai, D.-H. Lien, C.-Y. Huang, R.-H. Horng, and J.-H. He, "See-through Ga<sub>2</sub>O<sub>3</sub> solar-blind photodetectors for use in harsh environments," *IEEE Journal of Selected Topics in Quantum Electronics*, vol. 20, no. 6, p. 3802006, Nov./Dec. 2014.
- (72) G. Li, J. Zhang, and X. Hou, "Temperature dependence of performance of ZnO-based metal-semiconductor-metal ultraviolet photodetectors," *Sensors and Actuators A*, vol. 209, no. 1, pp. 149-153, Mar. 2014.
- (73) S. I. Stepanov, V. I. Nikolaev, V. E. Bougrov, and A. E. Romanov, "Gallium oxide: properties and applications - a review." *Reviews on Advanced Material Science*, vol. 44, pp. 63-86, Jan. 2016.
- (74) R.-H. Hrong, Y.-Y. Zeng, W.-K. Wang, C.-L. Tsai, Y.-K. Fu, and W.-H. Kuo, "Transparent electrode design for AlGa<sub>N</sub> deep-ultraviolet light-emitting diodes," *Optics Express*, vol. 25, no. 25, pp. 32206-32213, Dec. 2017.
- (75) R. Zou, Z. Zhang, Q. Liu, J. Hu, L. Sang, M. Liao, and W. Zhang, "High detectivity solar-blind high-temperature deep-ultraviolet photodetector based on multi-layered (100) facet-oriented  $\beta$ -Ga<sub>2</sub>O<sub>3</sub> nanobelts," *Small*, vol. 10, no. 9, pp. 1848-1856, May 2014.
- (76) F. Alema, "Vertical solar blind Schottky photodiode based on homoepitaxial Ga<sub>2</sub>O<sub>3</sub> thin film," in *Proc. SPIE 10105, Oxide-based Materials and Devices VIII*, 2017, p. 101051M.
- (77) S. Ghose, "Growth and characterization of wide bandgap semiconductor oxide thin films," Ph.D. dissertation, Dept. of Materials Science, Engineering, and Commercialization, Texas State Univ., San Marcos, TX, 2017.
- (78) M. Ai, D. Guo, Y. Qu, W. Cui, Z. Wu, P. Li, L. Li, and W. Tang, "Fast-response solar-blind ultraviolet photodetector with a graphene/ $\beta$ -Ga<sub>2</sub>O<sub>3</sub>/graphene hybrid structure," *Journal of Alloys and Compounds*, vol. 692, pp. 634-638, Jan. 2017.



- (79) H. O. Pierson, "Structure and Properties of Diamond and Diamond Polytypes," in *Handbook of carbon, graphite, diamonds and fullerenes: processing, properties and applications*, 1st ed. Park Ridge, New Jersey.
- (80) M. Liao, L. Sang, T. Teraji, M. Imura, J. Alvarez, and Y. Koide, "Comprehensive investigation of single crystal diamond deep-ultraviolet detectors," *Japanese Journal of Applied Physics*, vol. 51, no. 9R, p. 090115, Aug. 2012.
- (81) S. Salvatori, F. Scotti, G. Conte, and M. C. Rossi, "Diamond-based UV photodetectors for high-temperature applications," *Electronics Letters*, vol. 35, no. 20, pp. 1768-1770, Sep. 1999.
- (82) M. Rivera, R. Velazquez, A. Aldalbahi, A. F. Zhou, and P. Feng, "High operating temperature and low power consumption boron nitride nanosheets based broadband UV photodetector," *Scientific Reports*, vol. 7, p. 42973 Mar. 2017.
- (83) M. Rivera, R. Velazquez, A. Aldalbahi, A. F. Zhou, and P. X. Feng, "UV photodetector based on energy bandgap shifted hexagonal boron nitride nanosheets for high-temperature environments," *Journal of Physics D: Applied Physics*, vol. 51, no. 4, p. 045102, Jan. 2018.
- (84) W.-R. Chang, Y.-K. Fang, S.-F. Ting, Y.-S. Tsair, C.-N. Chang, C.-Y. Lin, and S.-F. Chen, "The hetero-epitaxial SiCN/Si MSM photodetector for high-temperature deep-UV detecting applications," *IEEE Electron Device Letters*, vol. 24, no. 9, pp. 565-567, Aug. 2003.
- (85) F.-R. Juang, Y.-K. Fang, Y.-T. Chiang, T.-H. Chou, and C.-I. Lin, "A high-performance n-i-p SiCN homojunction for low-cost and high-temperature ultraviolet detecting applications," *IEEE Sensors Journal*, vol. 11, no. 1, pp. 150-154, Jan. 2011.

- (86) T.-H. Chou, Y.-K. Fang, Y.-T. Chiang, C.-I. Lin, and C.-Y. Yang, "A low cost n-SiCN/p-SiCN homojunction for high temperature and high gain ultraviolet detecting applications," *Sensors and Actuators A*, vol. 147, no. 1, pp. 60-63, Sep. 2008.

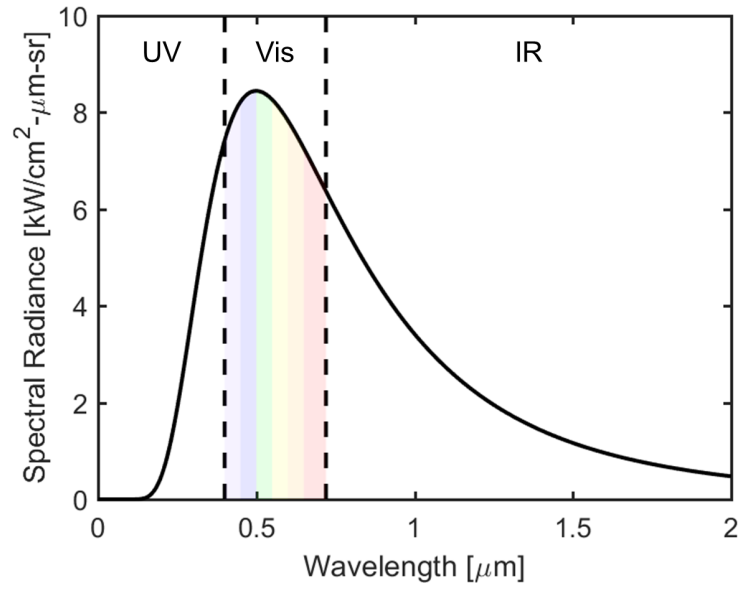


FIG 1. Black body radiation at 5800 K approximating the solar radiation spectrum outside Earth's atmosphere.

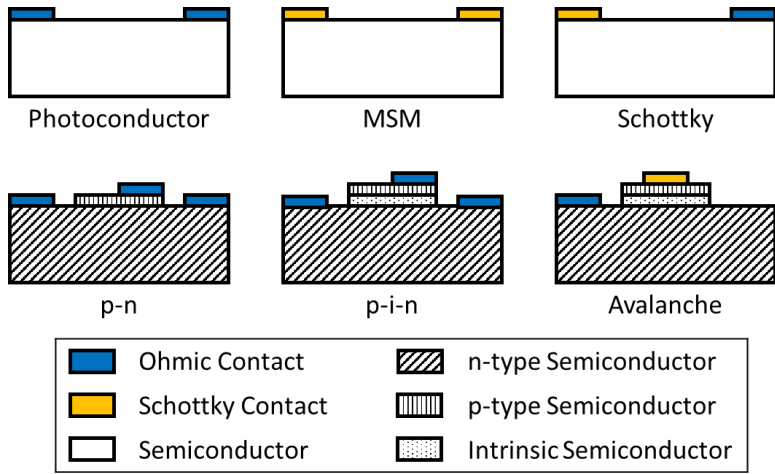


FIG 2. Different semiconductor photodetector device architectures.

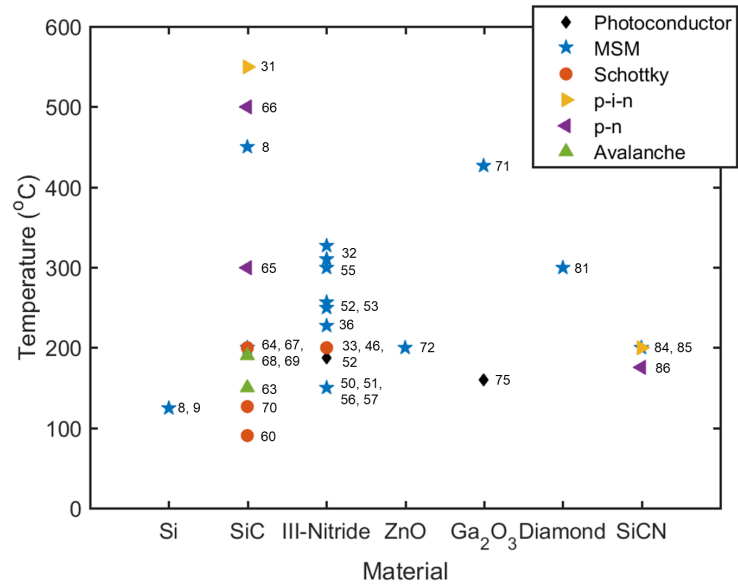


FIG 3. Maximum operational temperatures reported in literature for Si photodetectors compared to photodetectors based on wide bandgap materials.

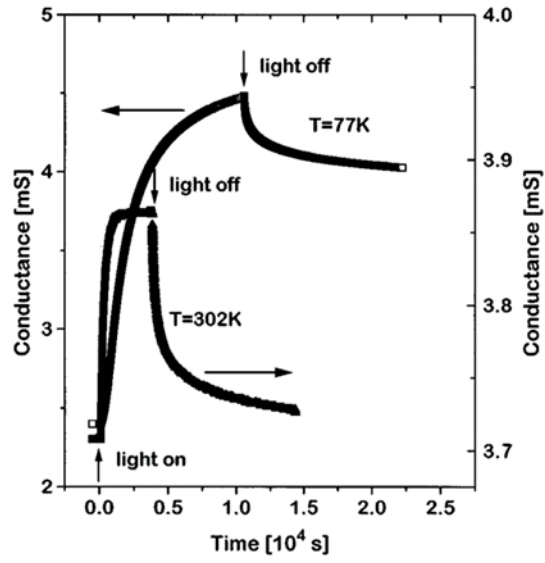


FIG 4. Buildup and decay transients of an n-type GaN substrate at 77 K and 302 K demonstrating decreased time constants at higher temperatures. Fig. 4 is adopted with permission from Ref. 37 (Copyright 1997, AIP Publishing).

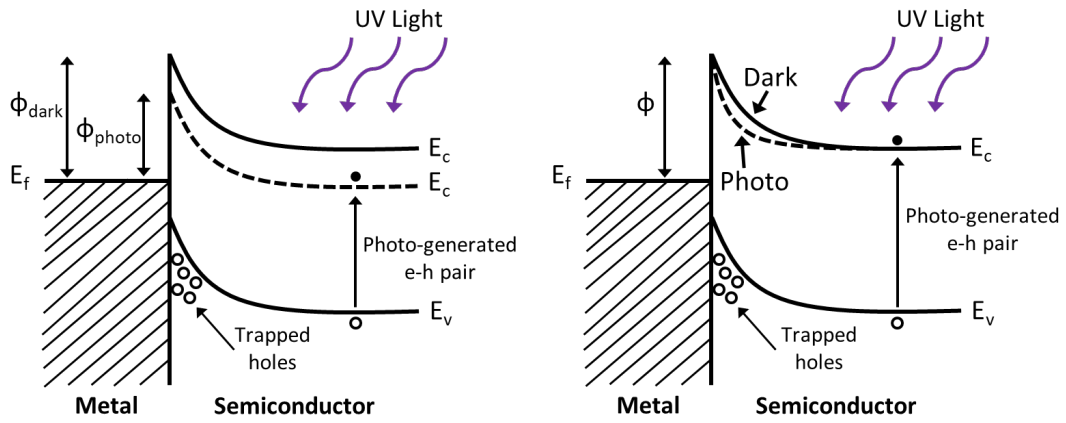


FIG 5. Trapped photo-generated holes lowering or bending the Schottky barrier with respect to the dark Schottky barrier.

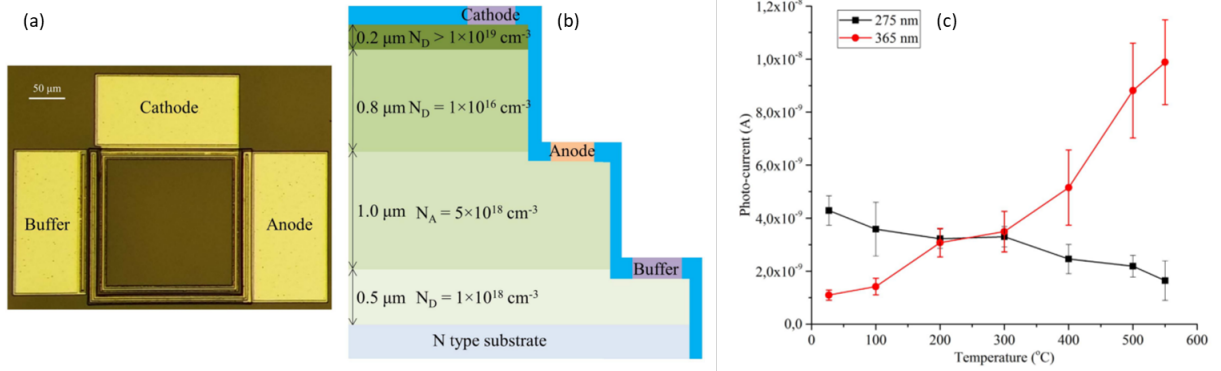


FIG 6. (a) Microscope image, (b) cross-section, and (c) photocurrent as a function of temperature for a SiC p-i-n photodetector. As temperature increases, the photocurrent generated by 275 nm light decreases while, the photocurrent generated by 365 nm light increases indicating bandgap narrowing at high temperature affects the photodetector response. Fig. 6 is adopted with permission from Ref. 31 (Copyright 2016, IEEE).



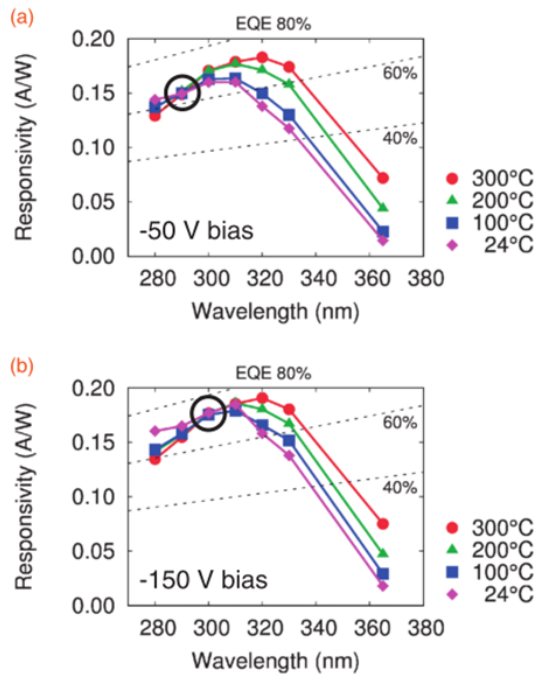
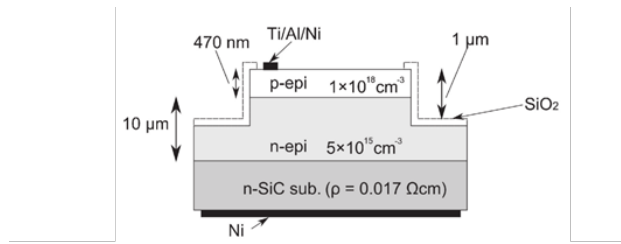


FIG 7. SiC p-n photodiodes demonstrating a temperature-independent photoresponse at a specific wavelength based on applied bias voltage. Fig. 7 is from Ref. 65 (Copyright 2012, IOP Publishing Ltd.).

TABLE I. Material properties of semiconductors used to manufacture UV photodetectors.

	<b>Si</b>	<b>AlN</b>	<b>Diamond</b>	<b>GaN</b>	<b>4H-SiC</b>	<b>6H-SiC</b>	<b>ZnO</b>
<b>Bandgap (eV)</b>	1.12 Indirect	6.2 Direct	5.5 Indirect	3.4 Direct	3.2 Indirect	2.86 Indirect	3.37 Direct
<b>Cut-off Wavelength (nm)</b>	1107	200	225	365	387	434	368
<b>Melting Point (°C)</b>	1410	2200	3500	2500	2700	2700	1975
<b>Thermal Conductivity (W/cm-K)</b>	1.5	3.2	20	1.3	4.9	4.9	5.4
<b>Electron Mobility (cm<sup>2</sup>/V-s)</b>	1400	135	2200	1000	400	400	205
<b>Hole Mobility (cm<sup>2</sup>/V-s)</b>	600	14	1600	30	75	75	70
<b>Dielectric Constant</b>	11.8	8.1	5.5	8.9	9.7	9.7	9.1
<b>Breakdown Field (10<sup>5</sup> V/cm)</b>	3	20	100	26	24	24	35

TABLE II. High temperature III-nitride-based UV photodetectors.

Material	Photodetector Architecture	Electrode Material	Temperature (°C)	PDCR	Responsivity (A/W)	Notes	Reference
GaN	MSM	Ti/Au	310		~8 (77°C) ~13 (310°C)	Thermal ionization of trapped photo-generated carriers increases responsivity.	32
GaN	MSM	Ni/Au	150		~0.1 (RT, 3V) ~0.04 (150°C, 3V)	Internal gain attributed to trapped photo-generated holes reducing the Schottky barrier height.	56
GaN		Al Wirebond	250	2.63 (RT, 1V) 0.27 (250°C, 1V)		Direct wirebonding. ZnO nanorods for antireflective coating.	54
GaN	MSM	Ni/Au	150			Dark current $\sim 10^{-12}$ A at RT and 150°C. Photocurrent $\sim 10^{-5}$ at RT and $\sim 10^{-6}$ at 150°C.	50
GaN	Photoconductor	Ti/Al or In	187			Very high gains ( $\sim 10^4$ at 187°C and $10^{-2}$ W/cm <sup>2</sup> optical power) attributed to a modulation mechanism of the conductive volume of the GaN layer.	46
GaN	MSM	Pt	257			Thicker GaN devices showed improved performance due to a reduction in defects and deep-level traps.	53
GaN	MSM	Ti/Au	227			Studied trapping mechanisms responsible for persistent photoconductivity.	36

AlGaN	MSM	Ni/Au	150		0.14 (RT, 10V) 0.11 (150°C, 10V)	Ultra-low dark current (fA range at 150°C) achieved using a high-temperature AlN buffer layer.	51
AlGaN	MSM	Ni/Au	150			QE: 11.3% (RT, 2V, front-illumination), 21.1% (RT, 2V, back-illumination)	57
InGaN	MIS	Ti/Al/Ni/Au Ni/WC	250	1317 (RT, -1V) 72 (250°C, -1V)	3.3 (RT, -3V) 5.6 (250°C, -3V)	UV/visible light discrimination ratio of $10^5$ at 250°C. Used CaF <sub>2</sub> insulation layer to reduce the dark current.	45, 52
InGaN	Schottky	Ti/Al/Ni/Au Ni/WC	200	79 (RT, -1V) 2.2 (200°C, -1V)			52
AlGaN/GaN	MSM	Ti/Au	327		~1 (27°C) ~18 (327°C)	Thermal ionization of trapped photo-generated carriers increases responsivity.	32
AlGaN/GaN	Photoconductor	Ti/Al/Pt/Au	200	1.4 (RT, 1V) 0.3 (200°C, 1V)	0.00035 (RT and 200°C, 1V)	V-grooved photodetector increases absorption of incident light resulting in higher sensitivity compared to planar photodetector.	33
AlGaN/GaN		Al Wirebond	100			Direct wirebonding enabling rapid fabrication and packaging. Signal to noise ratio: 29.2 (RT) and 14.4 (100°C)	34

AlGaIn/GaN		Ti/Al/Pt/Au	270 (Membrane Heating)	0.04 (RT, 30V)		Photocurrent decay time: 39 hours (1 V = membrane temperature 25°C) and 24 seconds (30 V = membrane temperature 270°C)	35
AlN	MSM	Ti/Pt	300	60 (RT, 5V) 3.5 (300°C, 5V)	0.015 (RT, 5V)	Rise time ~110 ms Decay time ~ 80ms	55

TABLE III. High temperature SiC-based UV photodetectors.

Material	Photodetector Architecture	Electrode Material	Temperature (°C)	PDCR	Responsivity (A/W)	Notes	Reference
4H-SiC	p-i-n	Ni Ni/Ti/Al	550	45.4 (500°C) 7.3 (550°C)	0.12 (RT) 0.046 (550°C)	From RT to 550°C, photocurrent increased by 9 times at 365 nm and decreased by 2.6 times at 275 nm due to bandgap narrowing.	31
4H-SiC	MSM	Cr/Pd	450	1.3 x 10 <sup>5</sup> (RT) 0.62 (450°C)	0.305 (RT, 20V)	Rise time: 594 μs (RT) and 684 μs (400°C) Fall time: 699 μs (RT) and 786 μs (400°C)	8
4H-SiC	Schottky	Ti/AlSiCu Ti/Ni/Au	90		0.046 (RT)	QE: 19% (RT)	60
4H-SiC	Avalanche	Ni/Ti/Al/Au	150		0.125 (RT)	Maximum QE: 53.4% (RT, 290 nm) and 63.3% (150°C, 295 nm)	63
4H-SiC	Avalanche	Ni/Ti/Al/Au	190		0.093 (RT)	QE: 41% (RT)	69
4H-SiC	p-n	Ti/Al/Ni	300		Between 0.15 and 0.2 (RT and 300°C)	Achieved a temperature independent photoresponse at targeted wavelengths by controlling the reverse bias voltage.	65
4H-SiC	Schottky	Ni/Ti/Al/Au Ni	200		0.115 (RT)	QE: 50% (RT) After thermal storage at 200°C in air for 100 hours, dark current increased slightly but remained less than 1 pA at 20 V.	64

4H-SiC	Schottky	Cr	127			QE: 26% (-198°C), 27.4% (102°C)	70
6H-SiC	n+-p	Ni Ti/Al	500		0.0586 (RT)	QE: 24.9% (RT) Photocurrent increased with increasing temperature.	66
Nanocrystalline SiC	MSM	Au	200	RT: 4.9, 13.3 (with ZnO Nanorods) 200°C: 4.9, 7.6 (with ZnO nanorods)		Used ZnO nanorod arrays as an antireflective coating.	67
$\beta$ -SiC on Porous Si	MSM	Al	200	30 (RT, 5V) 15 (200°C, 5V)	0.28 (RT, 5V) 0.25 (200°C, 5V)	High resistivity and flexible porous silicon substrate results in low dark current and improved high temperature performance.	68
$\beta$ -SiC on Si	MSM	Al	200	8 (RT, 5V) 1(200°C, 5V)	0.2 (RT, 5V) 0.17 (200°C, 5V)		68

---

TABLE IV. High temperature UV photodetectors from other wide bandgap materials.

Material	Photodetector Architecture	Electrode Material	Temperature (°C)	PDCR	Responsivity (A/W)	Notes	Reference
ZnO	MSM	Al	200		9 (RT) 2 (200°C)	Responsivity decreases with increasing temperature due to bandgap shrinkage and lattice scattering.	72
B-Ga <sub>2</sub> O <sub>3</sub>	MSM	IZO	427	14 (RT, 10V) 1.5 (427°C, 10V)	0.00032 (RT, 10V)		71
Ga <sub>2</sub> O <sub>3</sub> Nanobelt	Photoconductor	Au	160	72,463 (55°C, 20V) 8,892 (160°C, 20V)	870 (55°C, 20V) 650 (160°C, 20V)		75
Diamond	MSM	Ag	300			UV/visible (200-800nm) discrimination of four orders of magnitude up to 300°C.	81
BNNS		Au	400		9 μA/W (RT, 0V)	Photocurrent increased by a factor of four from RT to 400°C. Thermal noise increased by a factor of 3 from RT to 400°C.	82
SiCBN	MSM	Al	200	5.5 (RT) 2.5 (200°C)			9
SiCN	MSM	Au	200	6.5 (RT) 2.3 (200°C)			84
n-SiCN/i-SiCN/p-SiCN	n-i-p	Au	200	3180 (RT, -5V) 135.65 (200°C, -5V)	0.14 (RT, -5V)	QE: 67% (RT, -5V)	85
n-SiCN/i-SiCN/p-Si	n-i-p	Ni	200	60 (RT, -5V) 4.7 (200°C, -5V)			85



---

n-SiCN/p-SiCN	n-p	Ni Al	175	1940 (RT, -5V) 96.3 (175°C, -5V)	86
---------------	-----	----------	-----	-------------------------------------	----

---